Revision 2

Word count: 5421

Crystallization of bastnäsite and burbankite from carbonatite melt in the system $La(CO_3)F – CaCO_3 – Na_2CO_3$ at 100 MPa

Anna M. Nikolenko[1,2,3], Konstantin M. Stepanov[3,4], Vladimir Roddatis[1], Ilya V. Veksler[1,3]

[1] Helmholtz Centre Potsdam – German Research Centre for Geosciences GFZ, Telegrafenberg, 14473 Potsdam, Germany

[2] University of Potsdam, Institute of Geosciences, Karl-Liebknecht-Str. 24-25, 14476 Potsdam-Golm, Germany

[3] V.S. Sobolev Institute of Geology and Mineralogy SB RAS, Akad. Koptyuga, 3, Novosibirsk 630090, Russia

[4] Vereshchagin Institute for High Pressure Physics RAS, Troitsk, 142190 Moscow, Russia

Corresponding author: Anna M. Nikolenko (annanik@gfz-potsdam.de)

Konstantin M. Stepanov (stepanov@igm.nsc.ru)

Vladimir Roddatis (vladimir.roddatis@gfz-potsdam.de)

Ilya V. Veksler (veksler@gfz-potsdam.de)

Abstract

Bastnäsite [REE(CO_3)F] is the main mineral of REE ore deposits in carbonatites. Synthetic bastnäsite-like compounds have been precipitated from aqueous solutions by many different methods but previous attempts to model magmatic crystallization of bastnäsite from hydrous calciocarbonatite melts were unsuccessful. Here we present the first experimental evidence that bastnäsite and two other REE carbonates, burbankite and lukechangite, can crystallize from carbonatite melt in the synthetic system La(CO_3)F – $CaCO_3$ – Na_2CO_3 at temperatures between 580 and 850 °C and pressure 100 MPa. The experiments on starting mixtures of reagent-grade $CaCO_3$, Na_2CO_3, $La_2(CO_3)_3$ and LaF_3 were carried out in cold-seal rapid-quench pressure vessels. The studied system is an isobaric pseudoternary join of a quinary system where CO_2 and fluorides act as independent components. Liquidus phases in the run products are calcite, nyerereite, Na carbonate, bastnäsite, burbankite solid solution $(Na,Ca)_3(Ca,La)_3(CO_3)_5$ and lukechangite $Na_3La_2(CO_3)_4F$. Calcite and bastnäsite form a eutectic in the boundary join La(CO_3)F – $CaCO_3$ at 780 ± 20 °C and 58 wt% La(CO_3)F. Phase equilibria in the boundary join La(CO_3)F – Na_2CO_3 are complicated by peritectic reaction between Ca-free endmember of burbankite solid solution petersenite (Pet) and lukechangite (Luk) with liquid (L):

$Na_4La_2(CO_3)_5$ (Pet) + NaF (L) = $Na_3La_2(CO_3)_4F$ (Luk) + Na_2CO_3 (Nc)

The righthand-side assemblage becomes stable below 600 ± 20 °C. In ternary mixtures, bastnäsite (Bst), burbankite (Bur) and calcite (Cc) are involved in another peritectic reaction:

2 La(CO_3)F (Bst) + $CaCO_3$ (Cc) + 2 Na_2CO_3 (L) = $Na_2CaLa_2(CO_3)_5$ (Bur) + 2 NaF (L)

Burbankite in equilibrium with calcite replaces bastnäsite below 730 ± 20 °C. Stable solidus assemblages in the pseudoternary system are: basnäsite-burbankite-fluorite-calcite, basnäsite-burbankite-fluorite-lukechangite, bastnäsite-burbankite-lukechagite, burbankite-lukechangite-

nyerereite-calcite and burbankite-lukechangite-nyerereite-natrite. Addition of 10 wt% $Ca_3(PO_4)_2$ to one of the ternary mixtures resulted in massive crystallization of La-bearing apatite and monazite, and complete disappearance of bastnäsite and burbankite. Our results confirm that REE-bearing phosphates are much more stable than carbonates and fluorocarbonates. Therefore, primary crystallization of the latter from common carbonatite magmas is unlikely. Possible exceptions are carbonatites at Mountain Pass that are characterized by very low P_2O_5 concentrations (usually at or below 0.5 wt%) and extremely high REE contents in the order of a few weight percent or more. In other carbonatites, bastnäsite and burbankite probably crystallized from highly concentrated alkaline carbonate-chloride brines that have been found in melt inclusions and are thought to be responsible for widespread fenitization around carbonatite bodies.

Keywords: experimental petrology, carbonatite melts, REE ore deposits, Mountain Pass, Bayan Obo.

This is the peer-reviewed, final accepted version for American Mineralogist, published by the Mineralogical Society of America.
The published version is subject to change. Cite as Authors (Year) Title. American Mineralogist, in press.
DOI: https://doi.org/10.2138/am-2022-8064. http://www.minsocam.org/

61 ## Introduction

62 Mountain Pass in California, USA and Bayan Obo in China are the two world's largest
63 deposits of rare earth elements (REE) associated with carbonatites, and bastnäsite $REE(CO_3)F$ is
64 the main ore-forming mineral in both. Bastnäsite belongs to a group of fluorocarbonates
65 characterized by the general formula $n\ REE(CO_3)(F,OH) \cdot m\ CaCO_3$ where $m = 0$ (bastnäsite), or
66 1 (synchisite, parisite, röntgenite), and $n = 1$ (bastnäsite, synchisite), 2 (parisite), or 3
67 (röntgenite). The bastnäsite crystal structure is formed by REE-F layers parallel to the (001)
68 plane with triangular carbonate $(CO_3)^{2-}$ ions arranged between the layers. Other minerals of the
69 group have layers of Ca^{2+} ions alternating with the layers of REE-F (Donnay and Donnay, 1953).
70 In addition to Ca and REE, fluorocarbonates may contain major amounts of Na (arisite,
71 lukechangite), Ba (cordylite, cebaite) and other alkaline earth elements. Giant bastnäsite deposits
72 at Mountain Pass and Bayan Obo are hosted by very unusual carbonatites, but fluorocarbonates
73 of the bastnäsite group are also quite common in classical carbonatites that are related to silica-
74 undersaturated nephelinitic and melilititic magmas. In typical carbonatites, REE
75 fluorocarbonates are often associated with mixed carbonates such as calkinsite, carbocernaite,
76 ancylite, and the burbankite group minerals $(Na,Ca)_3(Ca,REE)_3(CO_3)_5$ (Belovitskaya and Pekov,
77 2004; Chakhmouradian and Zaitsev, 2012; Zaitsev et al., 2002). Because carbonatites are usually
78 strongly enriched in light rare earths, REE in minerals of the bastnäsite and burbankite groups
79 are mostly represented by Ce, La, Nd and Pr (in this order of decreasing natural abundance)
80 (Fleischer, 1978; Williams-Jones and Wood, 1992).

81 Since the first successful hydrothermal synthesis of bastnäsite in the 1950s (Jansen et al.,
82 1959), hydroxy- and fluorobastnäsite compounds have been precipitated from aqueous solutions
83 by different methods at atmospheric and elevated pressure (Haschke 1975; Hsu 1992; Pradip et

al., 2013; Shivaramaiah et al., 2016). Interest in bastnäsite-type compounds has been growing in recent decades owing to their use as starting materials for production of rare earth oxycarbonates ($REE_2O_2CO_3$) and oxyfluorides (REEOF), which are excellent host matrices for phosphorus used in optical technologies (Janka and Schleid, 2009; Lee and Jung, 2013), and also for production of CeO_2 nanoparticles (Montes-Hernandez et al., 2016). According to Haschke (1975), synthetic $La(CO_3)(OH)$ loses H_2O and CO_2 at ambient pressure between 425 and 525 °C to form $La_2O_2CO_3$, which subsequently decomposes to La_2O_3 between 625 and 800 °C. Decomposition of synthetic $La(CO_3)F$ at atmospheric pressure occurs between 520 and 550 °C with the formation of fluoroxide LaOF. Thermal stability of La-bastnäsite increases at P_{CO2} = 100 MPa to 810 °C for $La(CO_3)(OH)$ and 860 °C for $La(CO_3)F$ (Hsu, 1992). Experiments by Rowland (2017) and Rowland et al. (2020) showed that a further increase of pressure up to 1 GPa does not seem to significantly increase the thermal stability of $La(CO_3)F$ and the decomposition temperature remains between 850 and 900 °C.

In summary, bastnäsite-like compounds have been routinely synthetized by different methods in hydrothermal experiments but it has not been shown yet whether bastnäsite can crystallize from carbonate melt at conditions relevant for natural carbonatite magma. Jones and Wyllie (1983, 1986) and Wyllie et al. (1996) experimented on La-bearing carbonatite melts in the system $CaCO_3$ - $Ca(OH)_2$ - $La(OH)_3$ at 100 MPa but lanthanum hydroxide was the only La crystalline phase found in the run products. Wyllie et al. (1996) briefly mentioned that they had observed co-crystallization of calcite and hydroxybastnäsite from La-rich carbonatite melt in the system $CaCO_3$ – $Ca(OH)_2$ – $La(CO_3)(OH)$ between 550 and 630 °C but a detailed account of the experiments has not been published. Experiments on more complex compositions in the system $CaCO_3$ – $BaSO_4$ – CaF_2 – $Ca(OH)_2$ – $La(OH)_3$ that were designed to model crystallization of

carbonatitic melts that may have been parental to the Mountain Pass REE deposit (Jones and Wyllie, 1986; Wyllie et al., 1996) also did not produce bastnäsite. Lanthanum hydroxide was again the only La phase stable at temperatures up to 710 °C, and above that temperature it was replaced by oxyfluoride LaOF.

Notably, previous experimental studies universally used synthetic calciocarbonate melts with large amounts of H_2O in order to low crystallization temperatures down to a geologically realistic level. However, a growing amount of geological and experimental evidence (Kjarsgaard, 1998; Kjarsgaard et al., 1995; Nabyl et al., 2020; Wiedendorfer et al., 2017), and studies of melt inclusions (Guzmics et al., 2015; Nielsen et al., 1997; Panina, 2005; Sokolov et al., 1999; Veksler et al., 1998) imply that common carbonatite melts associated with nephelinitic and melilititic rocks contain variable but significant amounts of alkalis. Therefore, low crystallization temperatures of natural carbonatitic melts, down to about 560-600 °C, are probably due to the presence of alkali carbonate components rather than H_2O alone. Concentrations of total alkalis (Na_2O+K_2O) in carbonatite liquids at the start of magmatic crystallization of calcite are estimated to be somewhere between 5-20 wt% (Lee and Wyllie, 1998; Wiedendorfer et al., 2017), and fractional crystallization of calcite, apatite and minor silicates is expected to increase the alkali content in evolving carbonatite liquid up to 32-35 wt% characteristic for natrocarbonatite lava (Gittins and Jago, 1998; Wiedendorfer et al., 2017). All this evidence implies that common calciocarbonatites should probably be interpreted as calcite cumulates that have lost significant amounts of alkalis (especially Na) to fenitizing fluids expelled from evolving carbonatite magma at advanced stages of crystallization (Rankin, 2005 and references therein). Alkali loss from carbonatites has been documented by numerous field observations

since long ago (e.g., von Eckermann, 1966) and was tested experimentally (Veksler and Keppler, 2000).

In summary, a realistic experimental model of natural carbonatite liquid derived from nephelinitic magma at crustal pressure should crystallize calcite as a primary liquidus phase but contain major amounts of alkali carbonate components. Here we present first experimental evidence for crystallization of bastnäsite and burbankite solid solutions from carbonatite melt in the system $La(CO_3)F - CaCO_3 - Na_2CO_3$. Lanthanum was chosen to represent REE because it is the second most abundant REE after Ce in carbonatites and, unlike the latter, has only one (trivalent) oxidation state that is most typical for rare earths. In addition, we have done a few pilot experiments on a four-component mixture containing 10 wt% $Ca_3(PO_4)_2$. The additional runs were done in order to study the effects of apatite and monazite crystallization on the stability of bastnäsite and burbankite. In the discussion we draw some implications for the formation of REE deposits in carbonatites.

Experimental and analytical methods

Starting mixtures were prepared from reagent-grade $CaCO_3$, Na_2CO_3, $La_2(CO_3)_3$, $Ca_3(PO_4)_2$ and LaF_3. Pure reagents were dried at 100 °C overnight, mixed under acetone in agate mortar and then dried again. First we prepared an equimolar mixture of $La_2(CO_3)_3$ and LaF_3 that is equivalent to stoichiometric $La_2(CO_3)F$, and then mixed it with various amounts of Na and Ca carbonates. We used 12 mixtures with concentrations of the $La_2(CO_3)F$ component ranging from 20 to 50 wt% including 4 binary mixtures $CaCO_3$ - $La_2(CO_3)F$ and Na_2CO_3 - $La_2(CO_3)F$ (see Table 1). We tried to keep our starting mixtures as dry as possible but because we obtained $La_2(CO_3)_3$ by controlled dehydration of a commercially produced (Sigma-Aldrich) crystal hydrate $La_2(CO_3)_3 \cdot xH_2O$, minor amounts of H_2O cannot be ruled out. Another potential source of

152 H_2O in run products is hydrogen diffusion through gold and platinum container walls during the
153 experiments (Brooker et al., 1998).

154 Experiments were conducted in rapid-quench cold-seal pressure vessels at the German
155 Research Centre for Geosciences (GFZ Potsdam). A detailed description of this type of the
156 vessels was presented by Matthews et al. (2003). The autoclaves at GFZ Potsdam are made of
157 the Ni–Cr alloy Vakumelt ATS 290-G (ThyssenKrupp AG). Temperature was measured by an
158 external Ni-CrNi thermocouple calibrated against the melting temperature of gold. Total error of
159 temperature measurements including the uncertainties due to the temperature gradients is
160 estimated to be ± 5 °C. Pressure was measured by transducers, and the results were checked
161 against a pressure gauge. The transducers and gauge were factory-calibrated and have an
162 accuracy of better than ± 0.1 MPa. About 20-30 mg of starting materials were loaded into gold or
163 platinum capsules, 3 mm in outer diameter and 15 mm in length. Quenching of samples was
164 semi-isobaric and lasted a few seconds.

165 Run products were mounted in epoxy resin and polished using sandpaper and diamond
166 polishing pastes without water to avoid dissolution of alkali carbonates and other water-soluble
167 components. SEM images for preliminary identification of crystalline phases were collected
168 using back scattered electrons with a Quanta 3D field emission scanning electron microscope
169 (Thermo Fisher Scientific, former FEI) operated at 20 kV and equipped with an EDAX energy
170 dispersive spectrometer (EDS) Octane Elect Plus. The electron beam current was 4 or 8 nA. The
171 EDS detector was controlled by the TEAM software version 4.6.1. Major components in glass
172 and crystals were analyzed at the GFZ Potsdam using JEOL JXA-8230 Superprobe electron
173 microprobe and FEI Quanta 3D Dual Beam (SEM&FIB) was used for preliminary study of the
174 run products. The microprobe analyses were performed in WDS mode with accelerating voltage

of 15 kV and beam current of 5, 15 and 20 nA (the best results were obtained with 5 nA). Albite, dolomite, fluorite and monazite were used as standards for Na, Ca, F and La. To minimize the damage of carbonate phases by electron beam, we used defocused beam with a diameter from 20 to 40 μm.

Results

Run conditions and phase composition of run products are listed in Table 1; typical images of crystalline phases in ground and polished run products are presented in Figure 1, and a summary of electron microprobe analyses of individual phases is given in Tables 2 and 3. Vapor bubbles were observed in all the samples and free vapor phase, presumably dominated by CO_2, was universally present in addition to crystals and melt, as indicated in Table 1. As discussed below, interpretation of run products was greatly assisted by the unusual ability of La-rich carbonate melts for quenching to clear, transparent glass. Low viscosity of carbonatite melts ensured fast crystallization and reaction rates, even at temperatures around 600 °C. Crystal settling was commonly observed in vertically positioned capsules during our experiments.

As mentioned in the introduction, three experiments were carried out on a mixture with the addition of 10 wt% $Ca_3(PO_4)_2$ at 850, 750 and 700 °C (Table 1). Melts in these experiments did not quench to glass but formed fine-grained aggregates of dendritic crystals that are typical quench products of carbonatite and many other salt molten mixtures. Sample BCN-33 was completely crystallized at 700 °C to an aggregate of calcite, nyerereite, apatite and monazite.

Crystalline phases

Bastnäsite forms euhedral hexagonal plates up to 100 μm wide and about 10-20 μm thick (Fig. 1a, e and f). Its composition is relatively stable and close to the stoichiometric formula but

197 the measured F content is often lower than the theoretical value of 8.72 wt% (Table 2). The
198 lower F concentrations may be due to analytical errors or O^{2-} substituting for 2 F^{-}. Bastnäsite
199 contains minor amounts of Ca (0.3-1.3 wt% CaO) which probably substitutes for La in the
200 crystal structure. Sodium is below the detection limit in all the samples.

201 *Burbankite* in our experiments formed prismatic crystals, which were surrounded in some
202 samples by dendritic overgrowth (Fig. 1a, b, f-g). In the binary join Na_2CO_3 – $La(CO_3)F$
203 burbankite crystals are surrounded by liquid boundary layers enriched in Na and F were rims of
204 small, micrometer-sized dendritic crystals of Na carbonate formed upon quench (Fig. 1b).
205 Burbankite is a solid solution with a general formula $A_3B_3(CO_3)_5$. The A site in natural
206 burbankite is occupied by Na, Ca and may contain vacancies; the B site is filled by larger ions of
207 Sr, Ca, Ba, whereas REE can enter both sites, with preference to the B site (Belovitskaya and
208 Pekov, 2004). The composition of burbankite solid solution in our experiments varies broadly
209 from the Ca-free endmember petersenite $Na_3(NaLa_2)(CO_3)_5$ in the boundary system Na_2CO_3 -
210 $La(CO_3)F$ (run BCN-22 in Table 2) to equal molar amounts of Na and Ca and a vacancy in the A
211 site $(Na_2Ca\square)(CaLa_2)(CO_3)_5$ in ternary space with the $CaCO_3$ component. Mass concentration of
212 La_2O_3 in burbankite varies throughout the system from 38 to 46 %.

213 *Lukechangite* is a fluorocarbonate of Na and La with the ideal formula $Na_3La_2(CO_3)_4F$. It
214 is very rare in nature (Grice and Chao, 1997), but abundantly formed in association with
215 burbankite at 625 °C in sample BCN-18 and in association with Na carbonate natrite in run
216 BCN-37 at 580 °C. An alternative Na-La fluorocarbonate arisite (Piilonen et al., 2010) with the
217 formula $NaLa_2(CO_3)_3F$ clearly does not match the electron microprobe analyses (Table 2).
218 Lukechangite in sample BCN-18 contains 1.7 wt% CaO and in BCN-37 it is Ca-free.
219 Morphologically this phase is very distinct and much different from bastnäsite or burbankite

(Fig. 1c, d). It forms thin hexagonal plates measuring up to 500 μm in width and only 20-30 μm in thickness.

Calcite forms rounded oval crystals (Fig. 1e and f) with an average size broadly variable from run to run depending on the nucleation density. In the binary system $CaCO_3$ – $La(CO_3)F$, calcite contains less than 1 wt% La_2O_3 and it is compositionally close to the theoretical formula. In contrast, calcite crystallizing from ternary mixtures contains up to 8 wt% La_2O_3 and up to 1.8 wt% Na_2O. Calcite crystals in runs BCN-27 and -29 are strongly zoned from La-poor cores to La-rich rims. Linear correlation between La and Na concentrations corresponds to equimolar substitution of La^{3+} and Na^{+} for 2 Ca^{2+} in calcite crystal structure. Therefore, the calcite-melt distribution coefficient (D) for La primarily depends on Na/Ca ratio of the melt and it tends to decrease with falling temperature. It is only 0.004 in the Na-free run BCN-8; 0.4 in run BCN-24; and 0.1 in run BCN-27. Notably, the formation of REE-rich calcite was also observed by Mollé et al. (2021) in experiments involving complex Na-bearing carbonatite compositions.

Nyerereite is observed as large (up to 200x300 μm) subhedral prisms and rounded, anhedral aggregates (Fig. 1g, h). It contains up to 7.3 wt% La_2O_3 (Table 2) and Na slightly in excess of the ideal formula $Na_2Ca(CO_3)_2$. It appears that in this system nyerereite, like calcite, shows significant isomorphic substitution 2 $Ca^{2+} \rightarrow La^{3+} + Na^{+}$. The nyerereite/melt distribution coefficient for La varies in samples BCN-26 and BCN-34 between 0.28 and 0.37. Notably, natural nyerereite phenocrysts in natrocarbonatite lava have also shown high concentrations of REE (Zaitsev et al., 2009), and distribution coefficients comparable to those in our experiments.

Sodium carbonate (presumably natrite) formed rounded irregular drop-like and oval grains with an average size of about 150 μm (Fig. 1c and g). Run products containing this phase were very fragile, hygroscopic and unstable during grinding and polishing, but we managed to

prepare epoxy mounts of samples BCN-37 and BCN-38 suitable for microprobe analyses. According to the analyses, natrite in the Ca-free sample BCN-37 contains a few weight percent La_2O_3, and in sample BCN-38 it contains up to 10 wt% CaO and 3.2 wt% La_2O_3.

A few grains of *fluorite* were found in subsolidus of the $CaCO_3$ – $La(CO_3)F$ binary system in association with bastnäsite and calcite. According to electron microprobe analyses, fluorite composition is close to pure CaF_2 with only small amounts of La (around 0.2 wt% La_2O_3).

Fluorapatite in samples BCN-31 and BCN-32 formed numerous small rounded grains that are often too small for electron microprobe analyses. Fluorapatite crystals in BCN-33 are bigger, many of them are euhedral and up to 15-20 μm in size. The phase contains on average 2.1 wt% Na_2O and 4.7 wt% La_2O_3. This implies isomorphic substitution 2 $Ca^{2+} \rightarrow La^{3+} + Na^{+}$ that is characteristic for the natural phosphate mineral belovite-(La) belonging to the apatite supergroup (Kabalova et al. 1997).

Monazite in sample BCN-33 is observed as small euhedral prismatic crystals up to 10 μm in length. Its composition is close to the ideal formula $LaPO_4$.

Liquid phase and La solubility

Jones and Wyllie (1983) were probably the first who discovered that carbonate melts with high La content, in contrast to the vast majority of carbonatite liquids, quenched to homogenous glass at normal quenching rates used in experimental petrology. In our experiments, melts quenched to clear transparent glass in all the binary and ternary starting mixtures with 30-50 wt% of the $La(CO_3)F$ component. Melts with La_2O_3 contents below 20 wt% quenched to fine-

grained dendritic crystals of calcite and Na- and La-rich carbonate matrix that are typical for quenched carbonatite liquids (e.g., Fig. 1h).

The solubility of La in liquids saturated in bastnäsite and burbankite solid solution produced in our experiments depends on temperature and Na/Ca ratio of the melt composition. Notably, the two variables are interdependent as melt saturation in La minerals tends to be reached at lower temperature in compositions with high Na/Ca. Compositions most relevant for natural carbonatite magma are those that are saturated with both calcite and bastnäsite. A few samples meeting this requirement (Table 3) range from Na-free BCN-8 at 800 °C where La_2O_3 concentration in liquid is at 43.8 wt% to BCN-27 at 750 °C with La_2O_3 in the liquid at 19.7 wt% and the molar Na/Ca ratio of 2. Thus, La solubility in liquids saturated in calcite and bastnäsite tends to decrease with falling temperature and increasing Na/Ca in the liquid down to about 20 wt%. Liquid saturated in burbankite and nyerereite at 650 °C also contains 20 wt% La_2O_3 (sample BCN-34 in Table 3), so this solubility of La appears to be minimal for all the studied compositions. Notably, total REE concentration in bastnäsite-saturated multicomponent carbonatitic melt that modelled natural compositions in the experiments by Mollé et al. (2021) at 600 °C and 100 MPa was also at the level of approximately 20 wt. % La_2O_3.

Liquid compositions in phosphate-bearing samples BCN-31 and BCN-32 were not analyzed because of strong interference with small apatite crystals and the lack of crystal-free areas suitable for reliable microprobe analyses.

Phase equilibria in the system $La(CO_3)F – CaCO_3 – Na_2CO_3$

Solidus assemblages. As described in the previous section, burbankite, nyerereite and calcite in the $La(CO_3)F – CaCO_3 – Na_2CO_3$ ternary mixtures form solid solutions that contain significant

amounts of La but no detectable F. This and the presence of CO_2-dominated vapor implies that the system $La(CO_3)F$ – $CaCO_3$ – Na_2CO_3 at the conditions of our experiments is in fact a pseudoternary join of a five-component system where NaF and CO_2 are independent components. In Figure 2 we use trigonal-prismatic composition space for plotting the positions of all the mineral phases encountered in the studied part of the quinary system La^{3+} – Ca^{2+} – Na^+ – CO_3^{2-} – F^- and have connected equilibrium mineral assemblages with the Alkemade lines. For simplicity, minor compositional variations of calcite and nyerereite solid solutions are ignored and only burbankite is shown as a phase of variable composition.

According to the phase rule, the maximal number of crystalline phases that can be equilibrated with liquid and vapor in an isobaric quinary system is 4. The topology of phase equilibria shown in Figure 2 implies that the solidus mineral assemblages within the studied pseudoternary join are: bastnäsite-burbankite-fluorite-calcite, bastnäsite-burbankite-fluorite-lukechangite, bastnäsite-burbankite-lukechangite, burbankite-lukechangite-nyerereite-calcite and burbankite-lukechangite-nyerereite-natrite.

Liquidus equilibria. Triangular phase diagram in Figure 3 presents a projection of liquidus phase equilibria in the studied part of the pseudoternary system. Information on melting in the binary boundary join Na_2CO_3 – $CaCO_3$ at 100 MPa is taken from Cooper et al. (1975). Pure $Na_2Ca(CO_3)_2$ endmember nyerereite that melts congruently at 817 °C is an intermediate compound in the binary. Another intermediate compound shortite $Na_2Ca_2(CO_3)_3$ is stable only in subsolidus below 400 °C and is not shown in Figure 3. The extent of solid solutions (thick grey lines) is based on the electron microprobe data (Table 2). The compositions of burbankite *a* and *b* that coexist with calcite, nyerereite and lukechangite were determined by electron microprobe in samples BCN-29, BCN-34 and BCN-18 (Table 2). Unlike the diagram in Figure 2 that is

scaled in molar units, the pseudoternary join in Figure 3 is drawn in weight percent. One should also bear in mind that the solid solutions and some of the key Alkemade lines shown in Figure 3 lie off the plane of the join (see Fig. 2) and are projected onto it. The projection is done by recalculating mass concentrations of Na_2O, CaO and La_2O_3 determined for a given phase by electron microprobe to the normative components Na_2CO_3, $CaCO_3$ and $La(CO_3)F$, and normalizing the latter to 100%.

Mineral stability fields on the liquidus surface that were observed in the temperature interval between 580 and 850 °C are outlined and labeled in Figure 3 in red. The concentration of $La(CO_3)F$ component in our starting mixtures did not exceed 50 wt% and the most La-rich part of the join has not been studied. However, previous studies imply that the part of liquidus surface not covered by our experiments should be dominated by the stability field of LaOF that should replace bastnäsite above 860 °C (Hsu, 1992).

If a few fluorite crystals in subsolidus samples BCN-6 and BCN-23 are ignored (fluorite probably appeared because of a minor excess of LaF_3 over $La_2(CO_3)_3$ in the starting mixtures), liquidus relationships between calcite and bastnäsite in the boundary join $CaCO_3$ – $La(CO_3)F$ can be interpreted as a binary eutectic at 775 ± 20 °C and 58 wt% of the $La(CO_3)F$ component. Other minerals of the bastnäsite group (synchisite, parasite and röntgenite) did not form and are probably subsolidus phases. Phase relationships in the boundary join Na_2CO_3 – $La(CO_3)F$ are however more complex. Lukechangite (Luk), natrite (Nc) and Ca-free end-member of burbankite solid solution petersenite (Pet) are involved in a peritectic reaction with liquid (L):

$$Na_4La_2(CO_3)_5\ (Pet) + NaF\ (L) = Na_3La_2(CO_3)_4F\ (Luk) + Na_2CO_3\ (Nc)$$

The righthand-side assemblage becomes stable between 580 and 625 °C (samples BCN-22 and -37). The peritectic relationships between burbankite solid solution and lukechangite apparently extend to Ca-bearing ternary compositions.

Another peritectic reaction in the quinary composition space involves bastnäsite (Bst), calcite (Cc) and burbankite (Bur):

$$2\ La(CO_3)F\ (Bst) + CaCO_3\ (Cc) + 2\ Na_2CO_3\ (L) = Na_2CaLa_2(CO_3)_5\ (Bur) + 2\ NaF\ (L)$$

The equation implies that the assemblage Bst+Cc becomes unstable at a certain critical concentration of Na carbonate component in liquid, and bastnäsite is replaced by burbankite solid solution. The replacement of bastnäsite by burbankite in calcite-saturated compositions takes place approximately below 730 °C (see point *p1* in Fig. 3). Crystallization of burbankite, in turn, leads to accumulation of NaF component in melt. At advanced stages of crystallization and according to the first peritectic reaction, NaF component of the liquid and some burbankite react back and form lukechangite, e.g., in solidus assemblages with nyerereite and natrite. As shown in Figure 2, burbankite and lukechangite lie on the opposite sides of the studied pseudoternary join, and their liquidus relationships are difficult to plot in the projection. Nevertheless, liquid compositions in samples BCN-34 and BCN-38 (Table 3) give approximate positions of the "piercing points" *p2* and *p3*. Liquid of the composition *p2* should crystallize to solidus assemblage Bur+Nye+Cc+Luk, whereas on further cooling liquid *p3* should produce solidus assemblage Bur+Nye+Nc+Luk.

The effects of phosphate component

Starting mixture B18:C54:N18:CP10 (Table 1) initially contains 13.46 wt% La_2O_3, 4.58 wt% P_2O_5 and has the molar La/P = 1.28. Despite the significant molar excess of La over P and

352 extensive crystallization of apatite removing P_2O_5 together with CaO from the melt, La
353 carbonates and fluorocarbonates are totally absent from the solidus assemblage where La is
354 distributed between monazite and apatite, calcite and nyerereite solid solutions. As noted above,
355 solidus apatite contains 4.7 wt% La_2O_3, and the La_2O_3 concentrations in calcite and nyerereite
356 are 0.89 and 7.14 wt%, respectively. Our results confirm that REE phosphate minerals are much
357 more stable during magmatic crystallization than REE (fluoro)carbonate species, and at typical
358 concentrations of REE and P in carbonatite magma apatite and monazite should be the only
359 primary magmatic hosts of REE.

360 **Discussion**

361 This study is, to the best of our knowledge, the first experimental demonstration that
362 bastnäsite and burbankite can co-crystallize from carbonatite melt at P-T conditions relevant for
363 crustal carbonatite magmas. Our experiments show that fluorobastnäsite crystallize together with
364 burbankite and calcite from melts with low to moderate Na contents, whereas burbankite and
365 lukechangite completely replace bastnäsite in bulk compositions with Na/Ca molar ratio above 2.
366 The demonstration that bastnäsite and burbankite can readily crystallize from carbonate melt in
367 laboratory experiments on synthetic mixtures does not, however, prove the magmatic origin of
368 minerals in nature. Our experiments revealed two major obstacles for magmatic crystallization of
369 REE (fluoro)carbonates. The first is very high solubility of REE at about 15-20 wt% that was
370 also observed in previous studies (Jones and Wyllie, 1983, 1986; Wyllie et al., 1996). Such REE
371 concentrations are hardly reachable in natural carbonatite magmas. The second is much greater
372 stability of REE phosphate minerals at magmatic conditions in comparison with
373 (fluoro)carbonates, and high capacity of calcite and apatite for incorporating REE in their crystal
374 structures. It should be noted though that carbonatites at Mountain Pass are possibly a unique

375 exception in this respect. They are characterized by very low P_2O_5 concentrations, mostly below
376 0.5 wt% (Castor, 2008), and extreme enrichment in REE at a level that could have allowed
377 bastnäsite to out-compete REE-bearing phosphate minerals. However, the origin of such unusual
378 carbonatite magma is controversial. If Mountain Pass bastnäsite deposit is indeed magmatic, its
379 origin is possibly rooted in an exceptionally enriched mantle source (Poletti et al., 2016).

380 Carbonatite derivatives of nephelinitic-melilititic magmas that are most common have high
381 P/REE values that make primary magmatic crystallization of bastnäsite and burbankite very
382 unlikely if not impossible. Natrocarbonatite lava in this regard is an extreme and probably the
383 best studied example of derivative carbonatite produced from nephelinitic magma by a
384 combination of fractional crystallization and silicate-carbonate liquid immiscibility. The
385 concentrations of P_2O_5 and REE in natrocarbonatite are at about 0.75 wt% and 1800 ppm,
386 respectively (Keller and Spettel, 1995), and thus the molar REE/P is at about 0.12. This is ten
387 times lower than the La/P molar ratio in our phosphate-bearing mixture where bastnäsite and
388 burbankite were completely replaced by apatite and monazite.

389 However, as mentioned in the introduction, burbankite and bastnäsite are ubiquitous in
390 typical intrusive carbonatites. In some cases, burbankite has been observed to form large
391 (centimeter-sized), euhedral crystals that look like products of primary crystallization
392 (Chakhmouradian and Zaitsev, 2012). Therefore, there must be some way for REE in intrusive
393 carbonatites to bypass the phosphate precipitation and form carbonate minerals.

394 Traces of a possible parental media for precipitation of REE carbonates have been
395 probably found in fluid inclusions associated with plutonic carbonatites. Numerous studies (e.g.,
396 Bühn and Rankin, 1999; Bühn et al., 2002; Rankin, 2005; Walter et al., 2020) have reported
397 inclusions in minerals from carbonatites and their exocontact zones that contained highly

concentrated chloride-carbonate-sulfate brines with up to 3.7 wt% REE, 0.6-3 wt% F and no detectable phosphate. The brines are strongly enriched in alkalis and have been interpreted as fluids responsible for fenitization that is universally observed at contacts with intrusive carbonatites. If such fluids so enriched in REE are not expelled from carbonatite, they should be capable to form REE mineralization within carbonatite body. In good agreement with our experiments, burbankite (not bastnäsite) was found among the daughter minerals of the brine inclusions in association with Na bicarbonate nahcolite (Bühn and Rankin, 1999; Bühn et al., 2002). The content of H_2O in the fluid has been estimated at about 20 wt% and some researches prefer to call it a salt melt (Rankin, 2005). Such fluids or melts seem to be routinely produced by common intrusive carbonatites, possibly at the magmatic-hydrothermal transition.

Evidence is growing for an important role of hydrothermal fluids in the origin of the world's largest bastnäsite deposit at Bayan Obo in China (Yang et al., 2017 and references therein). Primary fluid inclusions are poorly preserved in Bayan Obo minerals but Fan et al. (2004, 2006) reported REE daughter minerals (presumably bastnäsite and cebaite) in inclusions of alkaline carbonate-chloride brines. Smith et al. (1999) described reaction textures in aegirine-magnetite-fluorite rocks and hydrothermally altered dolomite marble where monazite in immediate contact with calcite or dolomite had been replaced by fine-grained aggregate of bastnäsite and apatite. These observations imply that in hydrothermal systems at favorable conditions (high activities of F and carbonate ions, and elevated pH) bastnäsite can become more stable than monazite.

Implications

Despite liquidus crystallization of bastnäsite and burbankite in synthetic model system $La(CO_3)F - CaCO_3 - Na_2CO_3$, primary magmatic crystallization of REE carbonates and

fluorocarbonates from natural carbonatitic melts is unlikely (with a possible exception of the uniquely REE-rich and P_2O_5-poor carbonatites at Mountain Pass). The reason lies in much greater stability of REE-bearing phosphate minerals such as apatite and monazite at magmatic conditions. Carbonate and fluorocarbonate REE minerals in carbonatites are likely to crystallize from highly concentrated brines that are mostly composed of alkali carbonates, chlorides, sulfates and fluorides. Traces of such brines have been found in fluid inclusions, and the fluids are believed to be responsible for widespread fenitization of country rocks around carbonatite bodies. Studies of fluid inclusions demonstrated that the brines are capable to dissolve large amounts of REE (e.g., Bühn and Rankin, 1999; Rankin, 2005). The example of giant bastnäsite deposits at Bayan Obo in China shows that protracted fluid activity and multiple episodes of REE mobilization and redeposition may be required for bastnäsite accumulation at an economic level. Large body of thermodynamic and experimental data is available for chloride, fluoride and sulfate complexes of REE at hydrothermal conditions but information is sparse for carbonate complexes (Migdisov et al., 2016 and references therein). It is also not clear to what extent data on relatively dilute solutions is applicable to brines with characteristics approaching those of hydrated melts. Therefore, mechanisms behind the formation of alkaline carbonate-chloride brines in carbonatite systems, their properties and their role in transport and concentration of REE and other critical metals appear to be important and promising subjects for future research.

Acknowledgements

We thank Oona Appelt for help with EMP analyses of experimental products. Thoughtful and constructive reviews by Bruce Kjarsgaard, David Doleiš and an anonymous colleague inspired us to do additional experiments and improve the original version of the paper. The project was supported by RSF grant № 19-17-00013.

444

References

1. Belovitskaya, Y.V., and Pekov, I.V. (2004) Genetic mineralogy of the burbankite group. New Data on Minerals, 39, 50-64.
2. Brooker, R., Holloway, J. R., and Hervig, R. (1998) Reduction in piston-cylinder experiments: The detection of carbon infiltration into platinum capsules. American Mineralogist, 83 (9-10), 985-994.
3. Bühn, B., and Rankin, A.H. (1999) Composition of natural, volatile-rich Na–Ca–REE−Sr carbonatitic fluids trapped in fluid inclusions. Geochimica et Cosmochimica Acta, 63 (22), 3781-3797.
4. Bühn, B., Rankin, A.H., Schneider, J., and Dulski, P. (2002) The nature of orthomagmatic, carbonatitic fluids precipitating REE, Sr-rich fluorite: Fluid inclusions evidence from the Okorusu fluorite deposit, Namibia. Chemical Geology, 186, 75-98.
5. Castor, S.B. (2008) The Mountain Pass rare-earth carbonatite and associated ultrapotassic rocks, California. Canadian Mineralogist, 46, 779-806.
6. Chakhmouradian, A.R., and Zaitsev, A.N. (2012) Rare earth mineralization in igneous rocks: Sources and processes. Elements 8, 347-353.
7. Cooper, A.F., Gittins, J., and Tuttle, O.F. (1975) The system Na_2CO_3-K_2CO_3-$CaCO_3$ at 1 kilobar and its significance in carbonatite petrogenesis. American Journal of Science, 275, 534–560.
8. Donnay, G., and Donnay, J.D.H. (1953) The crystallography of bastnäsite, parisite, roentgenite, and synchisite. American Mineralogist, 38, 932-963.

9. Fan, H.R., Hu, F.F., Yang, K.F., and Wang, K.Y. (2006) Fluid unmixing/immiscibility as an ore-forming process in the giant REE–Nb–Fe deposit, Inner Mongolian, China: evidence from fluid inclusions. Journal of Geochemical Exploration, 89, 104-107.
10. Fan, H.R., Xie, Y.H., Wang, K.Y., Tao, K.J., and Wilde, S.A. (2004) REE daughter minerals trapped in fluid inclusions in the giant Bayan Obo REE-Nb-Fe deposit, Inner Mongolia, China. International Geology Review, 46, 638-645.
11. Fleischer, M. (1978) Relative proportions of the lanthanides in minerals of the bastnäsite group. Canadian Mineralogist, 16, 361–363.
12. Gittins, J., and Jago, B. C. (1998). Differentiation of natrocarbonatite magma at Oldoinyo Lengai volcano, Tanzania. Mineralogical Magazine, 62, 759-768.
13. Grice, J.D., and Chao, G.Y. (1997) Lukechangite-(Ce), a new rare-earth-fluorocarbonate mineral from Mont Saint-Hilaire, Quebec. American Mineralogist, 82, 1255-1260.
14. Guzmics, T., Zajacz, Z., Mitchell, R. H., Szabó, C., and Wälle, M. (2015) The role of liquid–liquid immiscibility and crystal fractionation in the genesis of carbonatite magmas: insights from Kerimasi melt inclusions. Contributions to Mineralogy and Petrology, 169(2), 17.
15. Gysi, A. P., and Williams-Jones, A. E. (2015) The thermodynamic properties of bastnäsite-(Ce) and parisite-(Ce). Chemical Geology, 392, 87–101.
16. Haschke, J.M. (I975) The lanthanum hydroxide fluoride carbonate system: The preparation of synthetic bastnäsite. Journal of Solid State Chemistry, 12, 115-121.
17. Hsu, L.C. (1992) Synthesis and stability of bastnäsites in a part of the system (Ce,La)-F-H-C-O. Mineralogy and Petrology, 47, 87–101.

18. Jago, B.C., and Gittins, J. (1991) The role of fluorine in carbonatite magma evolution. Nature, 349, 56–58.

19. Janka, O., and Schleid, T. (2009) Facile synthesis of bastnäsite-type $LaF[CO_3]$ and its thermal decomposition to LaOF for bulk and Eu^{3+}-doped samples. European Journal of Inorganic Chemistry, 3, 357–362.

20. Jansen, G.J., Magin, G.B., and Levin, B. (1959) Synthesis of bastnäsite. American Mineralogist, 44, 180–181.

21. Jones, A., and Wyllie, P. (1983) Low-temperature glass quenched from a synthetic, rare earth carbonatite: implications for the origin of the Mountain Pass deposit, California. Economic Geology, 78, 1721–1723.

22. Jones, A., and Wyllie, P. (1986) Solubility of rare earth elements in carbonatite magmas, indicated by the liquidus surface in $CaCO_3$-$Ca(OH)_2$-$La(OH)_3$ at 1 kbar pressure. Applied Geochemistry, 1, 95–102.

23. Kabalova, Y.K., Sokolova, E.V., and Pekov, I.V. (1997) Crystal structure of belovite-(La). Doklady Akademii Nauk, 355(2), 182-185.

24. Keller, J., and Spettel, B. (1995) The trace element composition and petrogenesis of natrocarbonatites. In K. Bell and J. Keller, Eds. Carbonatite Volcanism, p. 70-86. Springer, Berlin, Heidelberg.

25. Kjarsgaard, B.A. (1998) Phase relations of a carbonated high-CaO nephelinite at 0.2 and 0.5 GPa. Journal of Petrology, 39 (11-12), 2061-2075.

26. Kjarsgaard, B.A., Hamilton D.L., and Peterson T.D. (1995) Peralkaline nephelinite/carbonatite liquid immiscibility: comparison of phase compositions in

experiments and natural lavas from Oldoinyo Lengai. In K. Bell and J. Keller, Eds. Carbonatite volcanism, p. 163-190. Springer, Berlin, Heidelberg.

27. Lee, M.H., and Jung, W.S. (2013) Hydrothermal synthesis of $LaCO_3OH$ and Ln^{3+}-doped $LaCO_3OH$ powders under ambient pressure and their transformation to $La_2O_2CO_3$ and La_2O_3. Bulletin of the Korean Chemical Society, 34, 3609–3614.
28. Lee, W.-J., and Wyllie, P.J. (1998) Processes of crustal carbonatite formation by liquid immiscibility and differentiation, elucidated by model systems. Journal of Petrology, 39, 2005-2013.
29. Matthews, W, Linnen, R.L., and Guo, Q. (2003) A filler-rod technique for controlling redox conditions in cold-seal pressure vessels. American Mineralogist, 88, 701–707.
30. Mercier, N., Taulelle, F., and Leblanc, M. (1993) Growth, structure, NMR characterization of a new fluorocarbonate $Na_3La_2(CO_3)_4F$. European journal of solid state and inorganic chemistry, 30, 609-617.
31. Migdisov, A., Williams-Jones, A.E., Brugger, J., and Caporuscio, F.A. (2016) Hydrothermal transport, deposition, and fractionation of the REE: Experimental data and thermodynamic calculations. Chemical Geology, 439, 13-42.
32. Mollé, V., Gaillard, F., Nabyl, Z., Tuduri, J., Iacono-Marziano, G., Di Carlo, I., and Erdmann, S. (2021) Experimental crystallisation of a REE-rich calciocarbonatitic melt: crystallisation sequence and REE behaviour. EMPG-XVII Conference Abstracts, 61.
33. Montes-Hernandez, G., Chiriac, R., Findling, N., Toche, F., and Renard, F. (2016) Synthesis of ceria (CeO_2 and CeO_{2-x}) nanoparticles via decarbonation and Ce (III) oxydation of synthetic bastnäsite ($CeCO_3F$). Materials Chemistry and Physics, 172, 202-210.

533 34. Nabyl, Z., Massuyeau, M., Gaillard, F., Tuduri, J., Iacono-Marziano, G., Rogerie, G., Le
534 Trong, E., Di Carlo, I., Melleton, J., and Bailly, L. (2020) A window in the course of
535 alkaline magma differentiation conducive to immiscible REE-rich carbonatites.
536 Geochimica et Cosmochimica Acta, 282, 297-323.
537 35. Nielsen, T.F.D., Solovova, I.P., and Veksler, I.V. (1997) Parental melts of melilitolite and
538 origin of alkaline carbonatite: evidence from crystallised melt inclusions, Gardiner
539 complex. Contributions to Mineralogy and Petrology, 126, 331-344.
540 36. Panina, L.I. (2005) Multiphase carbonate-salt immiscibility in carbonatite melts: data on
541 melt inclusions from the Krestovskiy massif minerals (Polar Siberia). Contributions to
542 Mineralogy and Petrology, 150, 19-36.
543 37. Piilonen, P.C., McDonald, A.M., Grice, J.D., Cooper, M.A., Kolitsch, U., Rowe, R.,
544 Gault R.A., and Poirier, G. (2010) Arisite-(La), a new REE-fluorocarbonate mineral from
545 the Aris phonolite (Namibia), with descriptions of the crystal structures of arisite-(La)
546 and arisite-(Ce). Mineralogical Magazine, 74, 257-268.
547 38. Poletti, J.E., Cottle, J.M., Hagen-Peter, G.A., and Lackey, J.S. (2016) Petrochronological
548 constraints on the origin of the Mountain Pass ultrapotassic and carbonatite intrusive
549 suite, California. Journal of Petrology, 57, 1555-1598.
550 39. Pradip, Li, H.C.C., and Fuestenau, D.W. (2013) The synthesis and characterization of
551 rare earth fluorcarbonates. KONA Powder and Particle Journal, 30, 193–200.
552 40. Rankin, A.H. (2005) Carbonate-associated rare metal deposits: composition and
553 evolution of ore-forming fluids – the fluid inclusions evidence. In R.L. Linnen and I.M.
554 Samson, Eds, Rare-Element Geochemistry and Ore Deposits. GAC Short Course Notes,
555 17, p. 299-314.

556 41. Rowland II, R.L. (2017) Phase equilibria, compressibility, and thermal analysis of
557 bastnaesite-(La). PhD Thesis, University of Nevada, Las Vegas.
558 42. Rowland II, R.L., Lavina, B., Kaaden, K.E.V., Danielson, L.R., and Burnley, P.C. (2020)
559 Thermal analysis, compressibility, and decomposition of synthetic bastnäsite-(La) to
560 lanthanum oxyfluoride. Minerals, 10, 212.
561 43. Shivaramaiah, R., Anderko, A., Riman, R. E., and Navrotsky, A. (2016)
562 Thermodynamics of bastnäsite: A major rare earth ore mineral. American Mineralogist,
563 101 (5), 1129-1134.
564 44. Smith, M. P., Henderson, P., and Peishan, Z. (1999) Reaction relationships in the Bayan
565 Obo Fe-REE-Nb deposit Inner Mongolia, China: implications for the relative stability of
566 rare-earth element phosphates and fluorocarbonates. Contributions to Mineralogy and
567 Petrology, 134, 294-310.
568 45. Sokolov, S.V., Veksler, I.V., and Senin, V.G. (1999) Alkalis in carbonatite magmas: new
569 evidence from melt inclusions. Petrology, 7, 602-609.
570 46. Veksler, I.V., and Keppler, H. (2000) Partitioning of Mg, Ca, and Na between carbonatite
571 melt and hydrous fluid at 0.1–0.2 GPa. Contributions to Mineralogy and Petrology, 138,
572 27-34.
573 47. Veksler I.V., Nielsen T.F.D., and Sokolov S.V. (1998) Mineralogy of crystallized melt
574 inclusions from Gardiner and Kovdor ultramafic alkaline complexes: implications for
575 carbonatite genesis. Journal of Petrology, 39, 2015-2031.
576 48. Von Eckermann, H. (1966) Progress of research on the Alnö carbonatite. In O.F. Tuttle,
577 and J. Gittins, Eds., Carbonatites, p. 3-31. John Wiley and Sons, New York,

578 49. Walter, B.F., Steele-MacInnis, M., Giebel, R.J., Marks, M.A., and Markl, G. (2020)
579 Complex carbonate-sulfate brines in fluid inclusions from carbonatites: Estimating
580 compositions in the system H_2O-Na-K-CO_3-SO_4-Cl. Geochimica et Cosmochimica Acta,
581 277, 224-242.
582 50. Weidendorfer, D., Schmidt, M.W., and Mattsson, H.B. (2017) A common origin of
583 carbonatite magmas. Geology, 45 (6), 507-510.
584 51. Williams-Jones, A.E., and Wood, S.A. (1992) A preliminary petrogenetic grid for REE
585 fluorocarbonates and associated minerals. Geochimica et Cosmochimica Acta, 56, 725–
586 738.
587 52. Wyllie, P.J., and Tuttle O.F. (1960) The system CaO – CO_2 – H_2O and the origin of
588 carbonatites. Journal of Petrology, 1, 1-46.
589 53. Wyllie, P.J., Jones, A.P., and Deng, J. (1996) Rare earth elements in carbonate-rich melts
590 from mantle to crust. In A.P. Jones, F. Wall and C.T. Williams, Eds. Rare Earth Minerals:
591 Chemistry, Origin and Ore Deposits. Mineralogical Society UK Special Publications, 7,
592 Chapman & Hall, p. 77-103.
593 54. Yang, K.F., Fan, H.R., Santosh, M., Hu, F.F., and Wang, K.Y. (2011) Mesoproterozoic
594 carbonatitic magmatism in the Bayan Obo deposit, Inner Mongolia, North China:
595 constraints for the mechanism of super accumulation of rare earth elements. Ore Geology
596 Reviews, 40(1), 122-131.
597 55. Yang, X., Lai, X., Pirajno, F., Liu, Y., Mingxing, L., and Sun, W. (2017) Genesis of the
598 Bayan Obo Fe-REE-Nb formation in Inner Mongolia, north China craton: a perspective
599 review. Precambrian Research, 288, 39-71.

56. Zaitsev, A.N., Demény, A., Sindern, S., and Wall, F. (2002) Burbankite group minerals and their alteration in rare earth carbonatites—source of elements and fluids (evidence from C–O and Sr–Nd isotopic data). Lithos, 62, 15-33.

57. Zaitsev, A.N., Keller, J., Spratt, J., Jeffries, T.E., and Sharygin, V.V. (2009) Chemical composition of nyerereite and gregoryite from natrocarbonatites of Oldoinyo Lengai volcano, Tanzania. Geology of Ore Deposits, 51, 608-616.

Figure captions

Figure 1. Back-scattered electron images of experimental products. (a) Bastnäsite and burbankite in quenched glass (BCN-7); (b) prismatic burbankite crystals surrounded by boundary layers enriched in F and dendritic quench natrite (BCN-22); (c) natrite and lukechangite in sample BCN-37; (d) burbankite and lukechangite in sample BCN-18; (e) oval calcite grains and hexagonal plates of bastnäsite in glass (BCN-15); (f) burbankite, bastnäsite and minor calcite (BCN-19); (g), burbankite, nyerereite and natrite in sample BCN-38; (h) burbankite and nyerereite in sample BCN-34. Abbreviations for phases: Bst – bastnäsite, Bur – burbankite, Cc – calcite, Luk – lukechangite, Nc – natrite, Nye – nyerereite, L – liquid.

Figure 2. The positions of equilibrium crystalline phases and stable solidus assemblages plotted in the trigonal-prismatic compositional space $CaCO_3$ – Na_2CO_3 – $La_2(CO_3)_3$ – CaF_2 – NaF – LaF_3. The studied pseudoternary join $CaCO_3$ – Na_2CO_3 – $La(CO_3)F_2$ is shown as semi-transparent grey triangle. Phase compositions are plotted in molar units. The extent of burbankite solid solutions is shown by dotted line. Abbreviations for phases: Bst – bastnäsite, Bur – burbankite, Cc – calcite, Luk – lukechangite, Fl – fluorite, Nc – natrite, Nye – nyerereite.

624 **Figure 3**. Pseudoternary phase diagram of the system $CaCO_3$ – Na_2CO_3 – $La(CO_3)F_2$ at 100 MPa
625 in weight percent. The positions of starting mixtures are plotted as open circles. Primary
626 crystallization fields on liquidus surface are outlined and labeled in red. Red numbers are
627 temperature estimations in Centigrade. See text for discussion.
628

This is the peer-reviewed, final accepted version for American Mineralogist, published by the Mineralogical Society of America.
The published version is subject to change. Cite as Authors (Year) Title. American Mineralogist, in press.
DOI: https://doi.org/10.2138/am-2022-8064. http://www.minsocam.org/

Table 1. Run conditions and products.

Run#	Mixture*	T, C	P, MPa	Time, h	Run products**
BCN-1	B50:N50	750	100	19	L+V
BCN-2	B50:C50	750	100	19	Bst+Cc+V
BCN-3	B50:N50	700	100	21	L+V
BCN-4	B50:C50	700	100	21	Bst+Cc+V
BCN-5	B20:N80	750	100	72	L+Nc+V
BCN-6	B20:C80	750	100	72	Bst+Cc+ trace Fl+V
BCN-7	B50:C30:N20	750	100	72	L+Bst+Bur+V
BCN-8	B50:C50	800	100	20	L+Cc+V
BCN-9	B20:C80	800	100	20	L+Cc+V
BCN-12	B50:N50	650	100	69	L+V
BCN-13	B50:C30:N20	650	100	69	L+Bst+Bur+V
BCN-14	B50:C20:N30	700	100	42	L+Bur+V
BCN-15	B50:C30:N20	725	100	48	L+Bst +Bur+V
BCN-16	B50:C20:N30	650	100	20	L+Bur+minor Bst+V
BCN-18	B50:C20:N30	625	100	64	L+Bur+Luk+V
BCN-19	B50:C30:N20	625	100	64	L+Bst+Bur+Cc+V
BCN-20	B50:C20:N30	750	100	19	L+V
BCN-21	B50:C30:N20	800	100	19	L+V
BCN-22	B50:N50	625	100	23	L+Bur+V
BCN-23	B50:C50	775	100	19	Bst+Cc+ trace Fl+V
BCN-24	B20:C60:N20	850	100	48	L+Cc+V
BCN-25	B20:C40:N40	700	100	48	L+Nye+V
BCN-26	B20:C40:N40	650	75	42	L+Nye+V
BCN-27	B20:C60:N20	750	80	42	L+Cc+trace Bst+V
BCN-28	B50:C40:N10	750	100	64	L+Cc+Bst+V
BCN-29	B40:C40:N20	700	100	64	L+Cc+Bur+V
BCN-30	B30:C30:N40	700	100	64	L+V
BCN-34	B30:C30:N40	650	100	600	L+Nye+Burb+V
BCN-35	B40:C40:N20	650	100	26	L+Cc+Burb+V
BCN-37	B50:N50	580	100	48	L+Luk+Nc+V
BCN-38	B30:C20:N50	580	100	48	L+Bur+Nye+Nc+V
BCN-31	B18:C54:N18:CP10	850	100	72	L+Cc+Ap+V
BCN-32	B18:C54:N18:CP10	750	100	48	L+Cc+Ap+V
BCN-33	B18:C54:N18:CP10	700	100	120	Cc+Nye+Ap+Mnz+V

* Abbreviations for components: B – $La(CO_3)F$; C – $CaCO_3$; N – Na_2CO_3; CP – $Ca_3(PO_4)_2$. Numbers are concentrations of the components in weight percent.

** Abbreviations for phases: Ap – apatite, Bst – bastnäsite, Bur – burbankite, Cc – calcite, Fl – fluorite, Luk – lukechangite; Mnz – monazite, Nc – Na carbonate, Nye – nyerereite, L – liquid, V - vapor.

This is the peer-reviewed, final accepted version for American Mineralogist, published by the Mineralogical Society of America.
The published version is subject to change. Cite as Authors (Year) Title. American Mineralogist, in press.
DOI: https://doi.org/10.2138/am-2022-8064. http://www.minsocam.org/

635 Table 2. Typical compositions of crystal phases in experimental products*.

Phase	**Bastnäsite**				**Burbankite**				**Lukechangite**	**Calcite**			**Nyerereite**	
Sample	BCN-4	BCN-7	BCN-16	BCN-19	BCN-18	BCN-22	BCN-29	BCN-34	BCN-18	BCN-8	BCN-15	BCN-27	BCN-26	BCN-34
T, °C	700	750	650	625	625	625	700	650	625	800	700	750	650	650
La_2O_3 (wt%)	68.32	75.98	68.52	68.06	46.00	44.40	36.33	39.16	50.71	0.19	6.26	2.24	3.82	7.31
CaO	0.87	0.31	0.45	0.59	11.64	0.01	17.14	15.67	1.7	55.47	50.56	53.89	27.93	23.59
Na_2O	0	0	0.05	0	8.88	16.50	8.88	9.18	13.69	0.01	1.26	0.48	28.81	29.16
F	6.71	5.82	6.63	7.26	0.00	0.00	0.00	0.00	2.3	0.00	0.00	0.00	0.00	0.00
-O=2F	2.82	2.45	2.79	3.06	0.00	0.00	0.00	0.00	0.97	0.00	0.00	0.00	0.00	0.00
Total	73.08	79.67	72.86	72.86	66.52	60.91	62.35	64.02	68.39	55.67	58.1	56.61	59.51	60.05
La (apfu)	0.74	0.95	0.74	0.75	1.85	1.67	1.34	1.49	1.80	0	0.04	0.01	0.05	0.10
Ca	0.03	0.01	0.01	0.02	1.36	0.00	1.84	1.73	0.17	0.99	0.94	0.97	1.05	0.91
Na	0	0	0	0	1.87	3.26	1.72	1.83	2.55	0	0.04	0.02	1.97	2.04
F	0.63	0.62	0.62	0.68	0	0	0	0	0.70	0	0	0	0	0
C*	1.08	0.94	1.09	1.1	4.97	5.43	5.14	5.06	4.28	1.01	0.99	1	1.94	1.96
O	3	3	3.00	3	15	15	15	15	12	3	3	3	6	6

636 *Averages of multiple microprobe analyses (number of analyses from 5 to 10).

637 **Calculated assuming $[CO_2] = 100 - [Total]$, in weight percent.

638

This is the peer-reviewed, final accepted version for American Mineralogist, published by the Mineralogical Society of America.
The published version is subject to change. Cite as Authors (Year) Title. American Mineralogist, in press.
DOI: https://doi.org/10.2138/am-2022-8064. http://www.minsocam.org/

639 Table 3. Compositions of quenched liquids.

Run #	Mixture	T, °C	n	La_2O_3 (wt%)		CaO (wt%)		Na_2O (wt%)		F (wt%)		-O = 2F (wt%)	Total
				Av.	S.D.	Av.	S.D.	Av.	S.D.	Av.	S.D.		
BCN-8	B50:C50	800	6	43.76	0.49	25.49	0.19	0.00	0.00	5.60	0.31	2.36	72.49
BCN-7	B50:C30:N20	750	15	32.48	0.47	16.69	0.16	15.82	0.56	4.52	0.11	1.90	67.60
BCN-15	"	700	20	34.74	0.42	18.14	0.12	13.88	0.38	3.95	0.08	1.66	69.05
BCN-13	"	650	6	34.24	0.26	17.59	0.30	14.23	0.13	5.08	1.10	1.48	68.08
BCN-19	"	625	8	23.40	1.56	19.09	0.44	12.76	0.70	10.28	2.48	4.33	61.20
BCN-14	B50:C20:N30	700	25	35.06	0.33	11.63	0.07	20.20	0.49	3.62	0.11	1.52	68.98
BCN-16	"	650	24	31.69	0.61	12.64	0.13	22.21	0.72	5.10	0.16	2.15	69.50
BCN-18	"	625	21	29.29	0.78	15.14	0.16	21.85	0.75	5.38	0.19	2.27	69.40
BCN-28	B50:C40:N10	750	15	33.88	0.81	18.93	0.25	11.74	0.59	5.06	0.22	2.13	67.48
BCN-29	B40:C40:N20	700	15	29.18	0.65	16.30	0.51	18.43	0.59	4.21	0.29	1.77	66.35
BCN-35	"	650	15	27.07	1.02	17.32	0.69	18.65	1.64	5.05	0.23	2.12	65.96
BCN-34	B30:C30:N40	650	15	20.00	0.61	16.00	0.21	26.31	0.59	2.19	0.10	0.92	63.58
BCN-24	B20:C60:N20	850	20	16.47	0.27	25.38	0.66	21.08	0.85	2.18	0.11	0.92	64.19
BCN-27	"	750	20	19.66	0.50	20.72	0.72	23.01	1.08	2.54	0.18	1.07	64.85
BCN-25	B20:C40:N40	700	20	18.59	0.45	20.45	0.96	25.19	1.00	2.16	0.13	0.91	65.48
BCN-26	"	650	8	13.53	1.60	20.05	2.56	24.24	2.46	2.05	0.81	0.63	58.69
BCN-22	B50:N50	625	5	33.00	0.86	0.00	0.00	28.13	1.55	4.38	0.78	1.84	63.66
BCN-37	"	580	5	28.27	0.61	0.00	0.00	37.04	0.44	3.44	0.76	1.45	63.86
BCN-38	B30:C20:N50	580	7	23.04	0.10	10.67	0.12	37.91	0.91	3.10	0.22	1.31	70.31

640 Av. – average and S.D. – standard deviations of *n* microprobe analyses

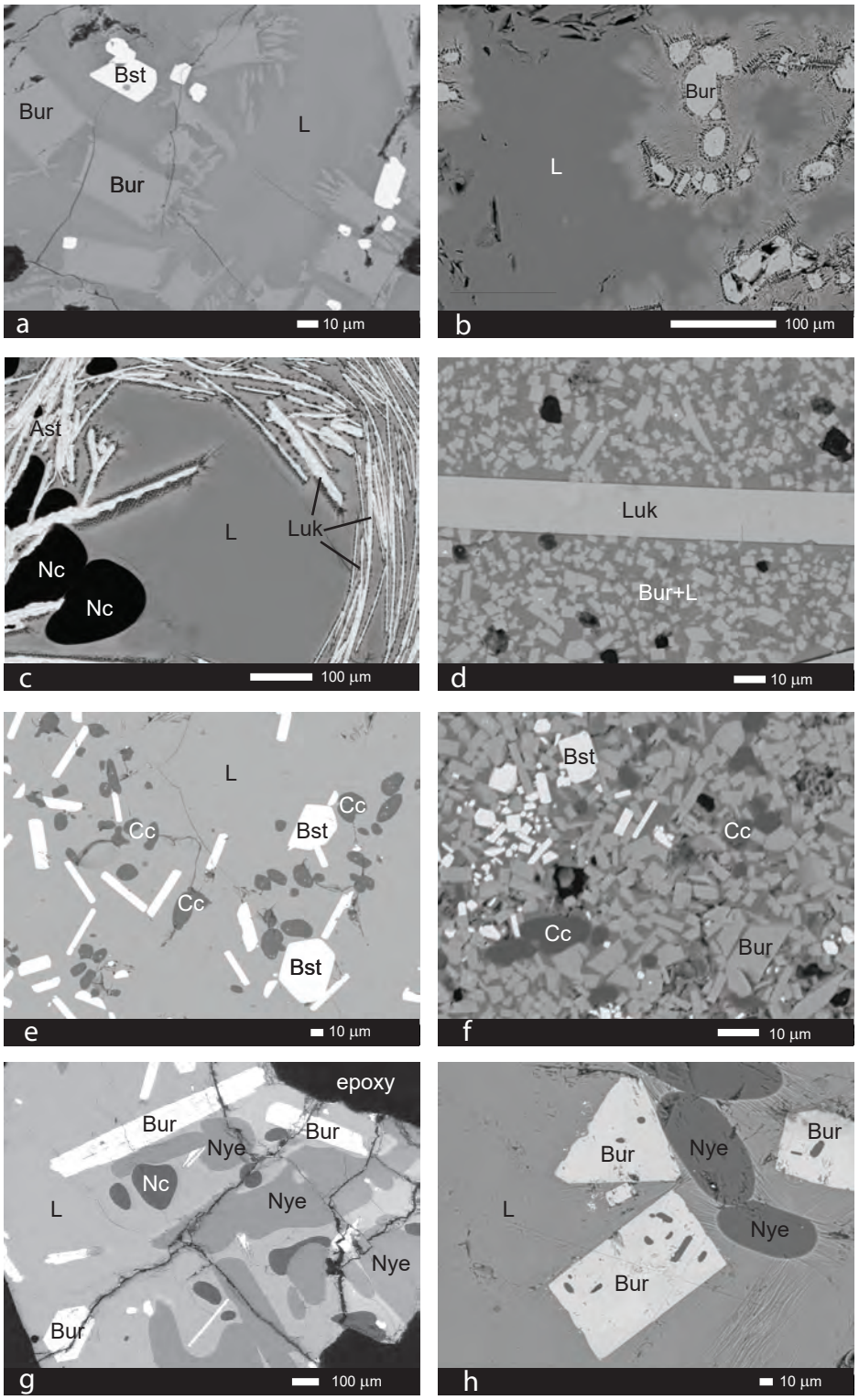

Fig. 1

This is the peer-reviewed, final accepted version for American Mineralogist, published by the Mineralogical Society of America.
The published version is subject to change. Cite as Authors (Year) Title. American Mineralogist, in press.
DOI: https://doi.org/10.2138/am-2022-8064. http://www.minsocam.org/

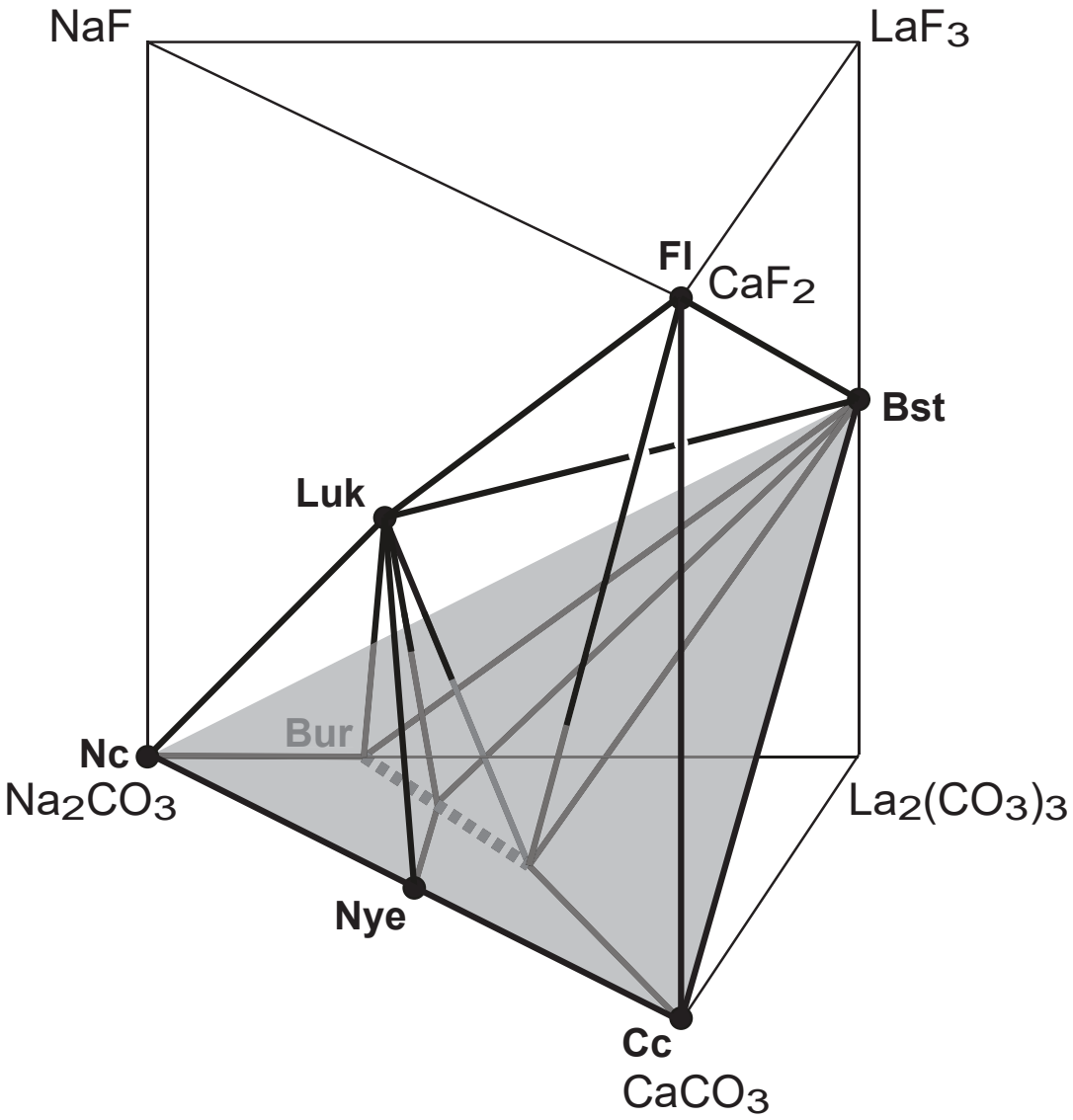

Fig. 2

This is the peer-reviewed, final accepted version for American Mineralogist, published by the Mineralogical Society of America.
The published version is subject to change. Cite as Authors (Year) Title. American Mineralogist, in press.
DOI: https://doi.org/10.2138/am-2022-8064. http://www.minsocam.org/

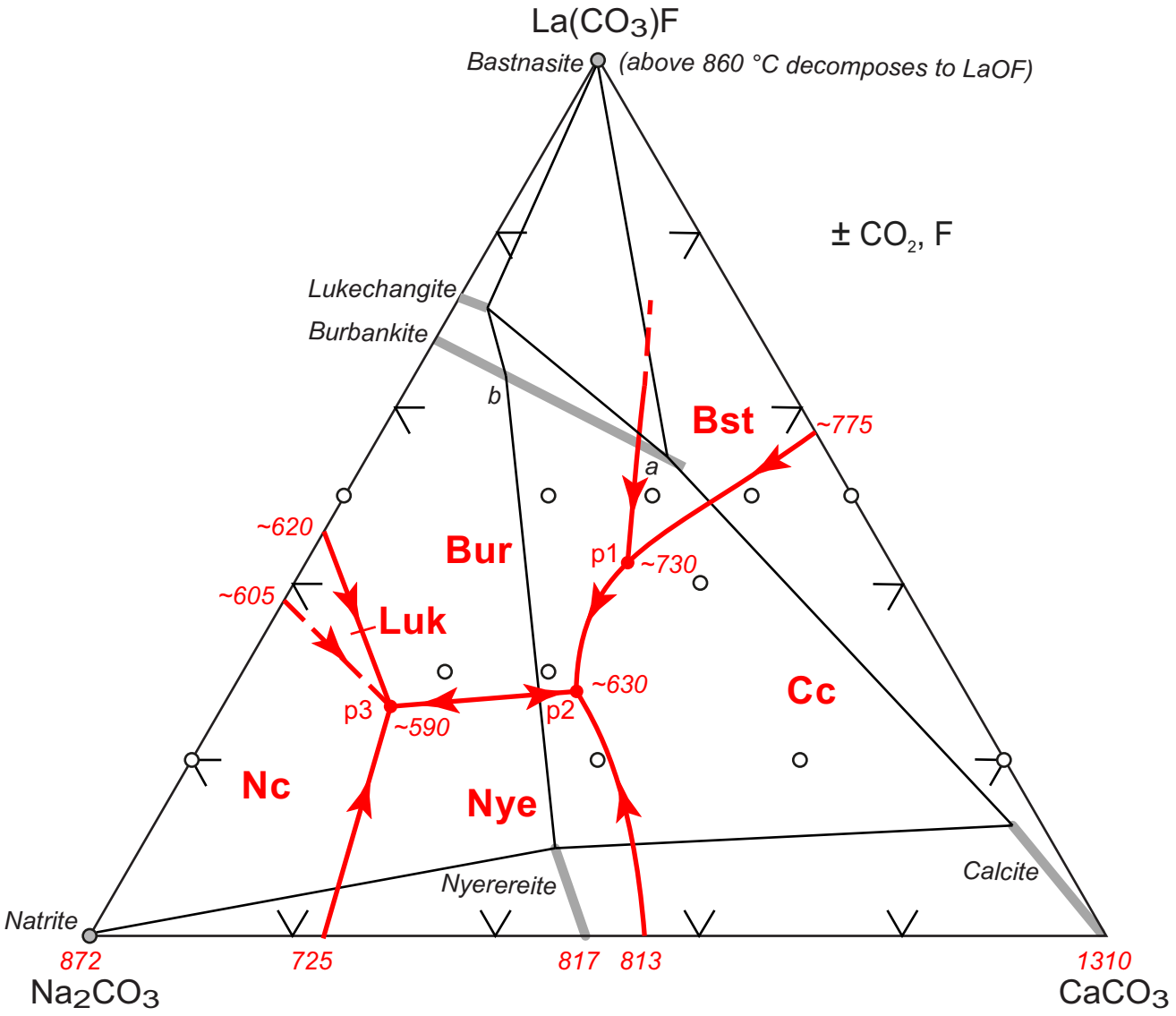

Fig. 3